FULL PAPER

Analogies between the topological insulator phase of 2D Dirac materials and the superradiant phase of atom-field systems

Manuel Calixto[1] ⓘ | Elvira Romera[2] ⓘ | Octavio Castaños[3] ⓘ

[1]Departamento de Matemática Aplicada and Instituto Carlos I de Fsica Teórica y Computacional (iC1), Facultad de Ciencias, Universidad de Granada, Granada, Spain

[2]Departamento de Fsica Atómica, Molecular y Nuclear and Instituto Carlos I de Fsica Teórica y Computacional (iC1), Universidad de Granada, 18071 Granada, Spain

[3]Instituto de Ciencias Nucleares, Universidad Nacional Autónoma de México, CDMX, Mexico

Correspondence
Manuel Calixto, Departamento de Matemática Aplicada and Instituto Carlos I de Fsica Teórica y Computacional (iC1), Facultad de Ciencias, Universidad de Granada, Fuentenueva s/n, 18071 Granada, Spain.
Email: calixto@ugr.es

Funding information
Agencia de Innovación y Desarrollo de Andalucía, Grant/Award Numbers: UHU-1262561, FQM-381, SOMM17/6105/UGR; Dirección General de Asuntos del Personal Académico, Universidad Nacional Autónoma de México, Grant/Award Number: DGAPA:IN101619; Ministerio de Ciencia e Innovación, Grant/Award Number: PGC2018-097831-B-I00

Abstract

A semiclassical phase-space perspective of band- and topological-insulator regimes of 2D Dirac materials and normal- and superradiant phases of atom-field interacting models is given in terms of delocalization, entropies, and quantum correlation measures. From this point of view, the low-energy limit of tight-binding models describing the electronic band structure of topological 2D Dirac materials such as phosphorene and silicene with tunable band gaps share similarities with Rabi-Dicke and Jaynes-Cummings atom-field interaction models, respectively. In particular, the edge state of the 2D Dirac materials in the topological insulator phase exhibits a Schrödinger's cat structure similar to the ground state of two-level atoms in a cavity interacting with a one-mode radiation field in the superradiant phase. Delocalization seems to be a common feature of topological insulator and superradiant phases.

KEYWORDS

atom-field interacting models, coherent states, edge and ground states, Husimi function, localization and entanglement measures, phase space, phosphorene, Schrödinger's cat, silicene, topological insulators, tunable band gap

1 | INTRODUCTION

Until quite recently, the Landau theory constituted the usual paradigm to describe phase transitions occurring at a critical point of some control parameters. Roughly speaking, this is based on the concept of "order parameter" (related to different organizations of the atoms or particles in the materials) that is finite in a broken symmetry phase. Different orders correspond to different symmetries in the organization of the constituent atoms (liquids, crystals, etc.). Gapless excitations (often called Goldstone modes) are a well-known consequence of the spontaneous symmetry breaking of a continuous underlying symmetry; for example, the spontaneous breakdown of the continuous translation symmetry of a liquid to the discrete symmetry of a crystal in solidification.

The Landau theory can be generalized to describe quantum-phase transitions (QPT), which are driven by quantum fluctuations as they take place at zero temperature. Examples of physical systems undergoing a QPT are: superconductor-insulator transitions, ferromagnets, radiation-matter interaction models, etc.[1,2] In this article, we shall pay attention to paradigmatic atom-field models displaying a superradiant phase above some critical value of the external electric field, for example, Rabi, Dicke, and Jaynes-Cummings (JC) models.[3,4] The JC model is a theoretical model of great interest to atomic physics, quantum optics, solid-state physics, and quantum information circuits, both experimentally and theoretically. It also has applications in coherent control and quantum information processing (see Greentree et al.[4] for a recent reference reviewing the physics of the JC model). Basically, it describes the system of a two-level atom interacting with a quantized mode of an optical cavity (a bosonic field) that can cause spontaneous emission and absorption. It was originally developed to study the interaction of atoms with the quantized electromagnetic field in order to investigate the phenomena of spontaneous emission and absorption of photons in a cavity.

Investigation of quantum critical phenomena beyond the Landau paradigm leads to topological-phase transitions (TPTs), which represent a new class of quantum critical phenomena. In fact, it is usually said that TPTs cannot be described within the usual framework of the Landau theory because they constitute a new kind of order that is beyond the usual symmetry description. Such is the case of chiral spin textures (in high-temperature superconductivity) and quantum Hall states with the same symmetry but different "topological order." In this article, we shall concentrate on 2D topological insulators (see References [5–7] for extensive reviews and Spencer and Morishita[8] for the special case of silicene), which are examples of "symmetry-protected topological order" (that respect time-reversal symmetries). Topological insulators have gapless boundary (edge) conducting states that are symmetry protected and dispersionless (robust against impurities and perturbations), similar to the quantum Hall effect. We shall concentrate on 2D materials of the graphene family, particularly silicene and phosphorene. They are two-dimensional allotropes of silicon and black phosphorus, respectively, with a hexagonal honeycomb structure similar to that of graphene but with a buckled structure that gives them a tunable band gap by applying external electric fields. They are also called Dirac materials because their low-energy (long wave length) effective electron dynamics can be described by a Dirac equation of electrons moving at the Fermi velocity. Unlike graphene, silicene and phosphorene can develop edge currents due to a nonzero spin-orbit coupling (nonzero Dirac mass gap), which plays the role of an "intrinsic" (vs external) magnetic field (when compared to the quantum Hall effect). These edge currents can be controlled by tuning the band gap (Dirac mass) by means of a perpendicular electric field applied to the material sheet, thus inducing transitions from a band (standard) insulator (BI) to a topological (edge conducting) insulator (TI) phase. TI-BI transitions can be characterized by the inversion of band together with a level crossing (edge states) at critical values of control parameters, and these topological phases are characterized by topological charges such as Chern numbers.[8] Their particular structure confers on Dirac materials interesting physical properties. In particular, it has been proposed that phosphorene can be used as a photodetector material[9] and in nanoelectronics within the framework of field effect transistor applications[10–12] because of its properties at room temperature. These are the band gap (up to 2 eV) and high carrier mobility ($1000 \, cm^2V^{-1}s^{-1}$). Actually, electronic devices have been manufactured using phosphorene with considerable success and good performance.[13–16]

Although topological and symmetry-breaking (Landau-like) quantum phases are different in nature, one can still identify some similarities between them, and this is one of the purposes of this article. We shall show that an information-theoretical analysis in the phase space of topological and standard quantum phases reveals a similar structure around the critical points, especially between edge and ground states. Actually, localization, entropy, and entanglement measures of Hamiltonian eigenstates have proven to be good markers of the QPT for the Dike model of matter-radiation interaction,[17–20] vibron model of molecules,[21–23] the ubiquitous Lipkin-Meshkov-Glick,[24–27] Bose-Einstein condensates,[28] bilayer quantum Hall effect,[29–31] etc. As shown in,[32] these entropic measures are even capable of identifying the order of the corresponding QPT. Inverse participation ratio and several kinds of entropies have also turned out to be useful to visualize the TI-BI transition in phosphorene[33] and silicene,[34–37] where entropy-based Chern-like numbers distinguishing TI and BI phases have been defined. In this article, we pay special attention to phosphorene, which has been less explored. We shall demonstrate that the low-energy (long wavelength) limit of tight-binding models of phosphorene and silicene share some similarities with traditional Rabi-Dicke and Jaynes-Cummings atom-field interaction models, respectively. There is a clear correspondence between the TI (resp. BI) regime of phosphorene and silicene and the superradiant (resp. normal) quantum phase of Rabi-Dicke and Jaynes-Cummings models. In particular, the edge state of the 2D Dirac materials in the topological insulator phase exhibits a Schrödinger's cat structure similar to the ground state of atom-field models in the superradiant phase. Therefore, delocalization seems to be a common feature of both kinds of phase transitions, and the extensive knowledge on Rabi-Dicke and Jaynes-Cummings models can help to better understand phosphorene and silicene, respectively.

The contribution is organized as follows: In Section 2, the low-energy Hamiltonian describing the properties of phosphorene in the presence of electric and magnetic fields is introduced together with the corresponding Hamiltonian for the better-known case of silicene. In Section 3, the eigenvalue problem for both Hamiltonians is solved, numerically for phosphorene and analytically for silicene, computing Landau levels and edge states and classifying them according to their symmetries (namely, parity). In Section 4, we introduce coherent states and the so-called Husimi function of pure states and reduced density matrices, which allows a visualization of quantum states in phase-space across the TI-BI transition in the vicinity of a critical point. We restrict ourselves in this case to phosphorene (silicene has been analyzed in[34]). In Section 5, we use information measures (moment of the Husimi distribution and Renyi-Wehrl entropy), which are good markers and descriptors of the TI-BI transition. In Section 6, we compare phosphorene and silicene with Rabi-Dicke and Jaynes-Cummings spin-boson models using the framework of coherent states. In particular, we show that edge states exhibit a Schrödinger's cat structure in the topological insulator phase, similar to the ground-state structure of atom-field systems in the superradiant phase. Finally, Section 7 is devoted to final conclusions.

2 | LOW-ENERGY MODEL HAMILTONIANS

We shall start discussing the less-known case of phosphorene. Phosphorene is a two-dimensional crystal of black phosphorus, similar to graphene, with a very stable orthorhombic structure (see Figure 1). This material has been studied both from an experimental and a theoretical point of view, and it has also been synthesized in a laboratory.[13,38–45]

A tight-binding Hamiltonian to describe the phosphorene electronic band structure has been proposed in Rudenko and Katsnelson[46] in the form

FIGURE 1 Phosphorene top view. Red (orange) thick points represent phosphorus atoms placed in the lower (upper) layer. The in-plane bond length is $a = 2.22$Å, and the in-plane bond angle is $\theta = 96.79°$. We represent the primitive vectors $a_x = 3.32$Å and $a_y = 4.38$Å by dashed arrows. The five solid arrows represent the first five neighbor hopping sites t_j necessary to describe phosorene, according to Rudenko and Katsnelson.[46]
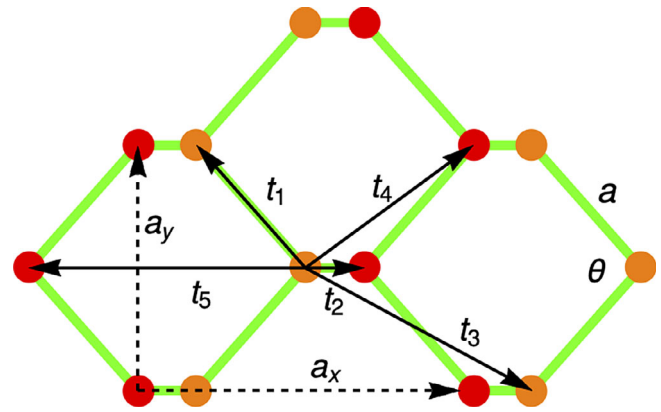
$$\tilde{H} = \sum_{\langle i,j \rangle} t_{ij} c_i^\dagger c_j, \tag{1}$$

where, as usual, t_{ij} is the transfer energy between lattice sites i and j, and $c_i^\dagger$, c_i are the creation and annihilation operators of electrons at position i, respectively. This model gives a band gap $E_g = 4t_1 + 2t_2 + 4t_3 + 2t_5$ for the five hopping links $t_1, ..., t_5$ of Figure 1.

After a second-order expansion around the Γ point of the Brillouin zone (k_x, k_y) and a minimal coupling to a perpendicular magnetic field $\mathbf{B} = (0, 0, B)$ to the phosphorene sheet [in the Landau gauge $\mathbf{A} = (-By, 0, 0)$], one arrives at the simplified Hamiltonian model (we refer the reader to References [33, 46–48] for more information)

$$\widehat{H}_B = \hbar\omega_\gamma \left(\widehat{a} + \widehat{a}^\dagger\right)\sigma_x + \frac{E_c + \hbar\omega_c\left(\widehat{a}^\dagger\widehat{a} + 1/2\right)}{2}(\sigma_0 + \sigma_z)$$

$$+ \frac{E_v - \hbar\omega_v\left(\widehat{a}^\dagger\widehat{a} + 1/2\right) - \left(\widehat{a}^2 + \widehat{a}^{\dagger 2}\right)\hbar\omega'}{2}(\sigma_0 - \sigma_z), \tag{2}$$

written in terms of Pauli matrices $\sigma_{x, y, z}$ plus identity σ_0 (two-band Hamiltonian) and the annihilation (and creation $\widehat{a}^\dagger$) operator

$$\widehat{a} = \sqrt{\frac{m_{cy}\omega_c}{2\hbar}}\left(y - y_0 + i\frac{\widehat{p}_y}{m_{cy}\omega_c}\right), \tag{3}$$

associated with the Landau sector and written in terms of an effective mass m_{cy}, the cyclotron frequency $\omega_c = eB/\sqrt{m_{cx}m_{cy}}$, the center $y_0 = \ell_B^2 k_x$, the magnetic length $\ell_B = \sqrt{\hbar/(eB)}$, the coordinate y, and the momentum $\widehat{p}_y$ (see References [33, 48] for more information). Moreover, ω_γ, ω_c, ω_v, and ω' are some effective frequencies (see Zhou et al.[48] for their values), and $E_c = 0.34$ eV and $E_v = -1.18$ eV are the conduction and valence energies, respectively, which give an energy gap of $E_g = E_c - E_v = 1.52$ eV.

In addition, we shall consider the application of a perpendicular electric field to the phosphorene sheet in the usual form $\widehat{H}_\Delta = \Delta\sigma_z$, with Δ being the electric potential. Therefore, the total phosphorene Hamiltonian will be

$$\widehat{H}_P = \widehat{H}_B + \widehat{H}_\Delta. \tag{4}$$

The electric field will be important in this problem as it provides a tunable band gap.

Similarly, the low-energy regime of a tight-binding model describing the electronic band structure of silicene under a perpendicular magnetic and electric field is reported by the 2D Dirac Hamiltonian (for simplicity, we restrict ourselves to the linear expansion around the K point of the Brillouin zone, and the fully polarized spin 1/2 case).[49–52]

$$\widehat{H}_S = \Delta_g \sigma_z + \hbar\omega\left(\widehat{a}\sigma_+ + \widehat{a}^\dagger \sigma_-\right), \tag{5}$$

where $\sigma_\pm = \frac{1}{2}(\sigma_x + i\sigma_y)$, $\omega = v\sqrt{2eB/\hbar}$ is the cyclotron frequency ($v = 5 \times 10^5$ m/s is the Fermi velocity), and the "Dirac mass" $\Delta_g = \frac{1}{2}\Delta + \frac{1}{2}\Delta_{so}$ provides a band gap, written in terms of the spin-orbit coupling $\Delta_{so} \simeq 4$ meV and the electric potential Δ. Later, in Section 6, we will comment on some similarities between the phosphorene $\widehat{H}_P$ and silicene $\widehat{H}_S$ low-energy Hamiltonians and the Rabi-Dicke and Jaynes-Cummings models for atom-field interaction, respectively.

3 | DIAGONALIZATION: PARITY SYMMETRY, LANDAU LEVELS, AND EDGE STATES

The basis states of the Hamiltonian (2) can be denoted by the ket $|k_x, n, s\rangle$, indicating the momentum k_x (the eigenvalue of $\hat{p}_x$), the Landau Level n (the eigenvalue of $\hat{n} = \hat{a}^\dagger \hat{a}$), and $s = \pm 1$ indicating the conduction and valence bands (the eigenvalues of σ_z). In the Landau gauge $\mathbf{A} = (-By, 0, 0)$, the eigenvectors can be written by

$$\langle xy | k_x, n+ \rangle = \frac{e^{ik_x x}}{\sqrt{L_x}} (\phi_n(y_c), 0)^T,$$
$$\langle xy | k_x, n- \rangle = \frac{e^{ik_x x}}{\sqrt{L_x}} (0, \phi_n(y_v))^T, \tag{6}$$

with

$$y_c = \sqrt{m_{cy}\omega_c/\hbar}(y - y_0), \quad y_v = \sqrt{m_{vy}\omega_v/\hbar}(y - y_0),$$

where ϕ_n are the wave functions of the harmonic oscillator. In the following analysis, we disregard the eigenvectors k_x of the momentum operator $\hat{p}_x$.

Due to the parity symmetry of Hamiltonian (2), $\hat{H}_P$ commutes with the parity operator $\hat{\Pi} = e^{i\pi \hat{n}_\sigma}$, with

$$\hat{n}_\sigma = \hat{n} + (\sigma_z + \sigma_0)/2,$$

implying that the matrix Hamiltonian is divided into two blocks associated with the even and odd parity solutions. Therefore, the k-th eigenstate (Landau level) is denoted by

$$|\psi_k\rangle = \sum_{n,s} c_{n,s}^{(k)} |n,s\rangle, \tag{7}$$

where the labels n and s of the expression are constrained to have $\pi(n, s) = \pm 1$; for conduction band, $k < 0$; and for valence band, $k > 0$. The matrix Hamiltonian for each sector is truncated to $n \leq N$ to achieve convergent results for the eigensystem for the given values of the magnetic and electric fields. Of course, the diagonalization of the matrices allows us to obtain the coefficients $c_{n,s}^{(k)}$.

In order to study the effect of a band inversion (TPT), we consider electric potentials around $\Delta \simeq -E_g = -1.52$ eV, that is, we analyze the range for the electric field interaction $-1.9 \leq \Delta \leq -1.0$ and for a magnetic field of $B = 20$T. The convergence is obtained for $N = 210$, and we have found that N must grow with $|\Delta|$ for $\Delta < -1.9$ (TI region) in order to achieve convergence. For other values of the magnetic field, similar qualitative results are obtained.

In Figure 2, the electronic band structure of phosphorene and silicene as a function of the electric potential Δ are exhibited for the first 13 low-energy LLs $k = -6, ..., 0, ..., 6$. There are six valence states (even and odd), six conduction states (even and odd), and the edge state $k = 0$ (black solid line). The edge state $k = 0$ suffers a band inversion around the critical value taken for the electric potential $\Delta_c = -E_g$ for phosphorene, while the value $\Delta_c = -\Delta_{so}$ for silicene. In both cases, one demonstrates that a topological transition occurs from a band insulator (BI) phase ($\Delta > \Delta_c$) to a topological insulator (TI) phase ($\Delta < \Delta_c$).

Note that the diagonalization of the Hamiltonian $\hat{H}_S$ in Equation (5) for silicene is easier and can be done analytically. This is so because the Hamiltonian possesses a larger symmetry, which makes the model integrable. Indeed, not only the parity $\hat{\Pi} = e^{i\pi \hat{n}_\sigma}$ but also the "total number of excitations" $\hat{n}_\sigma = \hat{n} + (\sigma_z + \sigma_0)/2$ commute with $\hat{H}_S$. Therefore, $\hat{H}_S$ and $\hat{n}_\sigma$ can be jointly diagonalized, with the corresponding Hamiltonian eigenvalues being.[49–52]

$$E_n = \begin{cases} \text{sgn}(n)\sqrt{|n|\hbar^2\omega^2 + \Delta_g^2}, & n \neq 0, \\ -\Delta_g, & n = 0, \end{cases} \tag{8}$$

and the Hamiltonian eigenvectors

$$|\psi_n\rangle = -ic_{n+}||n|-1,1\rangle + c_{n-}||n|,-1\rangle, \tag{9}$$

FIGURE 2 Low-energy spectra E_k of phosphorene (top panel, in eV units) and silicene (bottom panel, in Δ_{so} = 4 meV units) as functions of the electric field strength Δ for 13 LLs $k = -6, ..., 0, ..., 6$ (B = 20 T for phosphorene and B = 0.5 T for silicene). Valence (conduction) band LLs $k = -6, ..., -1$ ($k = 1, ..., 6$) are represented in red (blue) color (solid for even and dashed for odd parity). The edge state $k = 0$, represented in solid black, suffers band inversion around the critical electric potential $\Delta_c = -1.52$ eV for phosphorene and $\Delta_c = -\Delta_{so}$ for silicene (these transition points are marked with a vertical orange gridline). Even and odd parity LLs for phosphorene degenerate in the topological insulator region; in particular, the edge state degenerates with the odd parity conduction band LL $k = 1$ for $\Delta < \Delta_c$
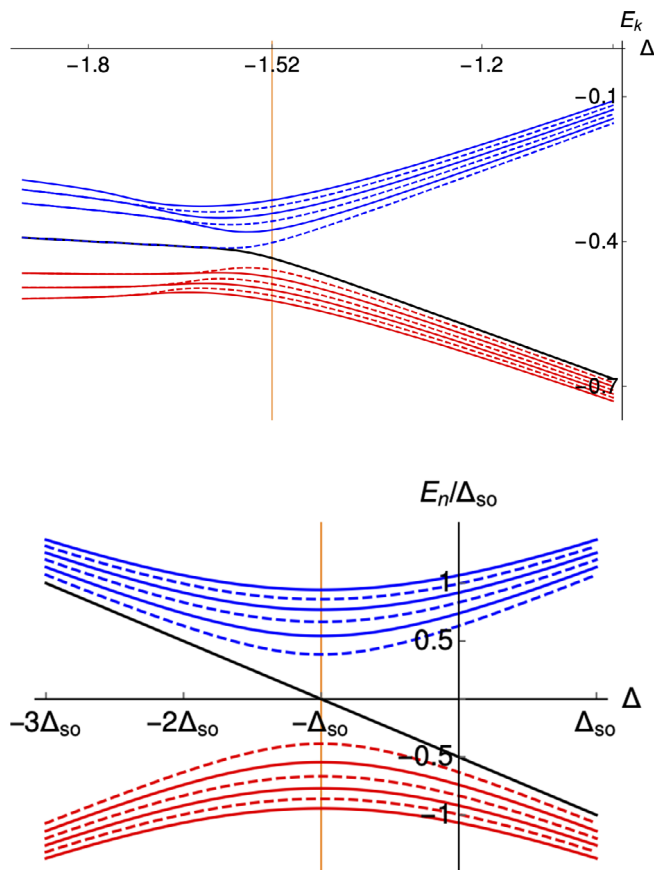
with coefficients

$$c_{n+} = \text{sgn}(n)\sqrt{\frac{|E_n| + \text{sgn}(n)\Delta_g}{2|E_n|}}, \quad n \neq 0, \tag{10}$$

$$c_{n-} = \sqrt{\frac{|E_n| - \text{sgn}(n)\Delta_g}{2|E_n|}}, \quad n \neq 0, \tag{11}$$

and $c_{0+} = 0$, $c_{0-} = 1$ for the edge state.

The structure of these first low-energy LLs for Silicene are displayed in Figure 2, where we have restricted ourselves to the even parity conduction $k = 6$ (solid blue) and valence $k = -6$ (solid red) eigenstates, together with the edge state $k = 0$ (solid black), as odd parity states display a similar behavior. We visualize the structure of these LLs in phase space, making use of the coherent state representation of $|\psi_k\rangle$, that is, the Husimi distribution function, and its moments, which turn out to be good markers of the BI-TI transition.

4 | COHERENT STATES, HUSIMI FUNCTION, AND REDUCED DENSITY MATRICES

Coherent states are usually obtained by applying a displacement operator (a unitary operation) on a highest/lowest weight state, namely, $|n\rangle \otimes |s\rangle = |0\rangle \otimes |-\rangle$. We have two kinds of coherent states associated with each sector. One is related to the oscillator or Landau sector

$$|\alpha\rangle = e^{\alpha a^\dagger - \bar{\alpha}a}|0\rangle = e^{-|\alpha|^2/2}\sum_{n=0}^{\infty}\frac{\alpha^n}{\sqrt{n!}}|n\rangle, \tag{12}$$

where $\alpha = q + ip$ is a complex number. The other is related to the band (spin) sector

$$|\theta,\phi\rangle = e^{\frac{\theta}{2}\left(e^{i\phi}\sigma_+ - e^{-i\phi}\sigma_-\right)}|-\rangle$$
$$= \cos\frac{\theta}{2}|-\rangle + e^{i\phi}\sin\frac{\theta}{2}|+\rangle, \tag{13}$$

where $\sigma_\pm = \frac{1}{2}(\sigma_x \pm i\sigma_y)$, and (θ,ϕ) are the polar and azimuthal angles on the Bloch sphere, respectively. These are the usual spin-$\frac{1}{2}$ SU(2) coherent states (the N-band case would require $SU(N)$ coherent states, in principle).

It is well known (see, eg, Perelomov[53]) that coherent states form an overcomplete set of the corresponding Hilbert space and fulfill the closure relations or resolutions of the identity:

$$1_L = \frac{1}{\pi}\int_{\mathbb{R}^2} d^2\alpha\,|\alpha\rangle\langle\alpha|,\ d^2\alpha = dqdp,$$
$$1_B = \frac{1}{2\pi}\int_R \sin\theta d\theta d\phi\,|\theta,\phi\rangle\langle\theta,\phi|,\ R = [0,\pi] \times [0,2\pi], \tag{14}$$

in the Landau (L) and band (B) sectors, respectively. The coherent state, or phase space, representation of a basis state $|n, s\rangle$ is then given by:

$$\varphi_{n,s}(\alpha;\theta,\phi) = \langle n|\alpha\rangle\langle s|\theta,\phi\rangle = \frac{e^{-\frac{|\alpha|^2}{2}}\alpha^n}{\sqrt{n!}}\frac{\left(\tan\frac{\theta}{2}e^{i\phi}\right)^{\frac{1+s}{2}}}{\sec\frac{\theta}{2}}. \tag{15}$$

The Husimi or Q-function of a normalized state $|\psi_k\rangle$ like (7) is defined as

$$Q_{\psi_k}(\alpha;\theta,\phi) = |\langle\alpha,\theta,\phi|\psi_k\rangle|^2$$
$$\sum_{n,n'}\sum_{s,s'} c^{(k)}_{ns}\bar{c}^{(k)}_{n's'}\varphi_{n,s}(\alpha;\theta,\phi)\bar{\varphi}_{n',s'}(\alpha;\theta,\phi), \tag{16}$$

and normalized according to:

$$\int_{\mathbb{R}^2 \times R} Q_{\psi_k}(\alpha,\theta,\phi)\frac{d^2\alpha\sin\theta d\theta d\phi}{2\pi^2} = 1. \tag{17}$$

We are interested in visualizing the Landau and band sectors separately. Therefore, we shall define the reduced density matrices of the Landau sector

$$\rho^L_{\psi_k} = \sum_{n,\bar{n}}\sum_s c^{(k)}_{ns}\bar{c}^{(k)}_{\bar{n}s}\,|n\rangle\langle\bar{n}| \tag{18}$$

and of the band sector

$$\left(\rho^B_{\psi_k}\right) = \begin{pmatrix} \varrho_{++} & \varrho_{+-} \\ \varrho_{-+} & \varrho_{--} \end{pmatrix} = \begin{pmatrix} \sum_n\left|c^{(k)}_{n+}\right|^2 & \sum_n c^{(k)}_{n+}\bar{c}^{(k)}_{n-} \\ \sum_n\bar{c}^{(k)}_{n+}c^{(k)}_{n-} & \sum_n\left|c^{(k)}_{n-}\right|^2 \end{pmatrix}. \tag{19}$$

Parity symmetry implies that $\varrho_{-+} = \varrho_{+-} = 0$. In Figure 3, we plot the populations ϱ_{++} and ϱ_{--} of three Landau levels $k = -6, 0, 6$ as a function of the electric potential Δ. The plot reflects the fact that $\varrho_{++} + \varrho_{--} = 1$, and therefore, they are symmetric with respect to the value 1/2. In the BI region ($\Delta \gg -1.52$ eV), the band populations of Hamiltonian eigenstates are polarized: $\varrho_{--} \simeq 1$ for edge and valence bands, and $\varrho_{++} \simeq 1$ for conduction band states, whereas in the TI region ($\Delta \ll -1.52$eV), we have $\varrho_{--} \simeq \varrho_{++}$ (balanced populations).

We are also interested in visualizing the corresponding "marginal" or reduced Husimi functions $Q^L_{\psi_k}(\alpha) = \left\langle\alpha|\rho^L_{\psi_k}|\alpha\right\rangle$ and $Q^B_{\psi_k}(\theta,\phi) = \left\langle\theta,\phi|\rho^B_{\psi_k}|\theta,\phi\right\rangle$. In Figure 4, the phase-space behavior of the Landau levels is exhibited by the Husimi function $Q^L_{\psi_k}(\alpha)$. One can see a transition from a bimodal regime to a unimodal regime. In addition, from the BI to the TI phases, there is a continuous delocalization of the Landau levels in phase space. We see in Figure 4 that the edge state $k = 0$ displays a "Schrödinger's cat structure" structure, that is, a quantum superposition of quasiclassical, macroscopically distinguishable (no overlapping) states (also called "parity-adapted coherent states"). This structure is shared

by the ground state of atom-field systems in the superradiant phase, as we show in Section 6. This delocalization property is quantified later on in Figure 6 by using the Husimi function second moment.

In Figure 5, we represent $Q_{\psi_k}^B(\theta,\phi)$ that, for Hamiltonian eigenvalues with defined parity, turns out to be independent of ϕ. We find that $Q_0^B(\theta) \simeq 0.5$ in the TI region, that is, the Husimi band distribution of the edge state, is quite uniform between the north ($\theta = 0$) and the south ($\theta = \pi$) poles of the Bloch sphere. This is consistent with Figure 3, where we found that $\varrho_{--} \simeq \varrho_{++}$ (balanced populations) for the edge state in the TI region. The analysis $Q^B(\theta)$ for the BI phase and for the valence and conduction states is also consistent with the results of the band populations in Figure 3.

5 | INFORMATION-THEORETIC ANALYSIS AND BI-TI TOPOLOGICAL TRANSITION

We have visualized the structure in phase space of the reduced density matrices $\rho_{\psi_k}^L$ and $\rho_{\psi_k}^B$ across the critical point Δ_c, observing a higher delocalization of the corresponding Husimi distributions in the TI phase. Now, we want to quantify this delocalization by using the ν-th moments of the reduced Husimi distributions of a state ψ

$$
\begin{aligned}
M_\psi^{L,\nu} &= \int_{\mathbb{C}^2} \frac{d^2\alpha}{\pi} Q_\psi^L(\alpha)^\nu, \\
M_\psi^{B,\nu} &= \int_R \frac{\sin\theta d\theta d\phi}{2\pi} Q_\psi^B(\theta,\phi)^\nu.
\end{aligned}
\tag{20}
$$

When $\psi = \psi_k$ is a Hamiltonian eigenstate, then the moments acquire an intrinsic dependence on the electric potential $M_{\psi_k}^{L(B),\nu}(\Delta)$ and will play the role of an order parameter for the TPT occurring at $\Delta_c = -E_g = -1.52$ eV, from the BI $\Delta > \Delta_c$ to the TI $\Delta < \Delta_c$ regime. The definition of the moment is not restricted to integer values of ν. Once $M_\psi^{L(B),\nu}$ are known for all integers ν, there is a unique analytic extension to complex (and therefore real) ν. The "classical" (vs quantum von Neumann) Rényi-Wehrl entropy is then defined as:

$$
W_\psi^{L(B),\nu} = \frac{1}{1-\nu} \ln\left(M_\psi^{L(B),\nu}\right),
\tag{21}
$$

which tends to the Wehrl entropy

$$
W_\psi^{L(B)} = -\int d\mu^{L(B)} Q_\psi^{L(B)} \ln Q_\psi^{L(B)}
\tag{22}
$$

when $\nu \to 1$, where $d\mu^L = d^2\alpha/\pi$ and $d\mu^B = \sin\theta d\theta d\phi/(2\pi)$. Among all moments, we shall single out the so-called "inverse participation ratio" (IPR) $M_\psi^{L(B),2}$, which somehow measures the inverse of the area (localization) occupied by $Q_\psi^{L(B)}$ in phase space. It is also related to the purity $P = \text{tr}(\rho^2)$ (the trace of the squared reduced density matrix) of the state and measures how entangled they are in the band (B) and the Landau (L) sectors across the TPT. The purity is related to the linear entropy by $S = 1 - P$. The maximum values of $M_{max}^{L,2} = \frac{1}{2}$ and $M_{max}^{B,2} = \frac{2}{3}$ are attained when $|\psi\rangle$ is itself a coherent state $|\alpha'; \theta', \phi'\rangle$ (minimal area). This is related to the Wehrl-Lieb's conjecture.[54,55] For the sake of convenience, we shall normalize the second moments in the Landau and band sectors according to $P_\psi^L \equiv 2M_\psi^{L,2}$ and $P_\psi^B \equiv \frac{3}{2}M_\psi^{B,2}$, respectively, in order to set the maximum IPR values to
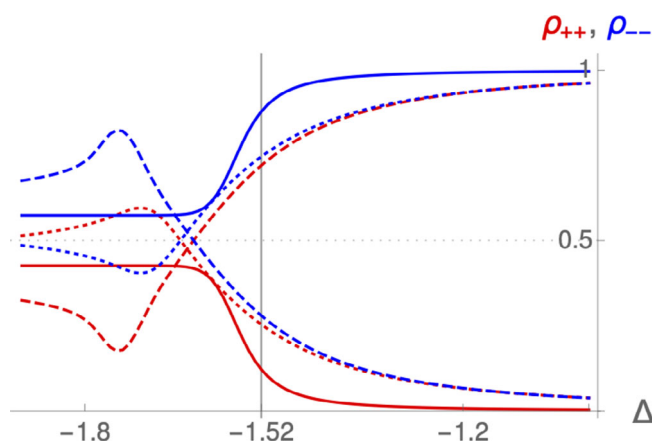
FIGURE 3 Diagonal components ϱ_{++} (red) and ϱ_{--} (blue) of the reduced density matrix $\left(\rho_{\psi_k}^B\right)$ for three Landau levels, $k = -6$ (valence band, dotted), $k = 0$ (edge state, solid), and $k = 6$ (conduction band, dashed), as a function of the electric potential Δ. The critical point $\Delta_c = -1.52$ eV, separating the band ($\Delta > \Delta_c$) from the topological insulator ($\Delta < \Delta_c$) regime, is marked with a vertical grid line
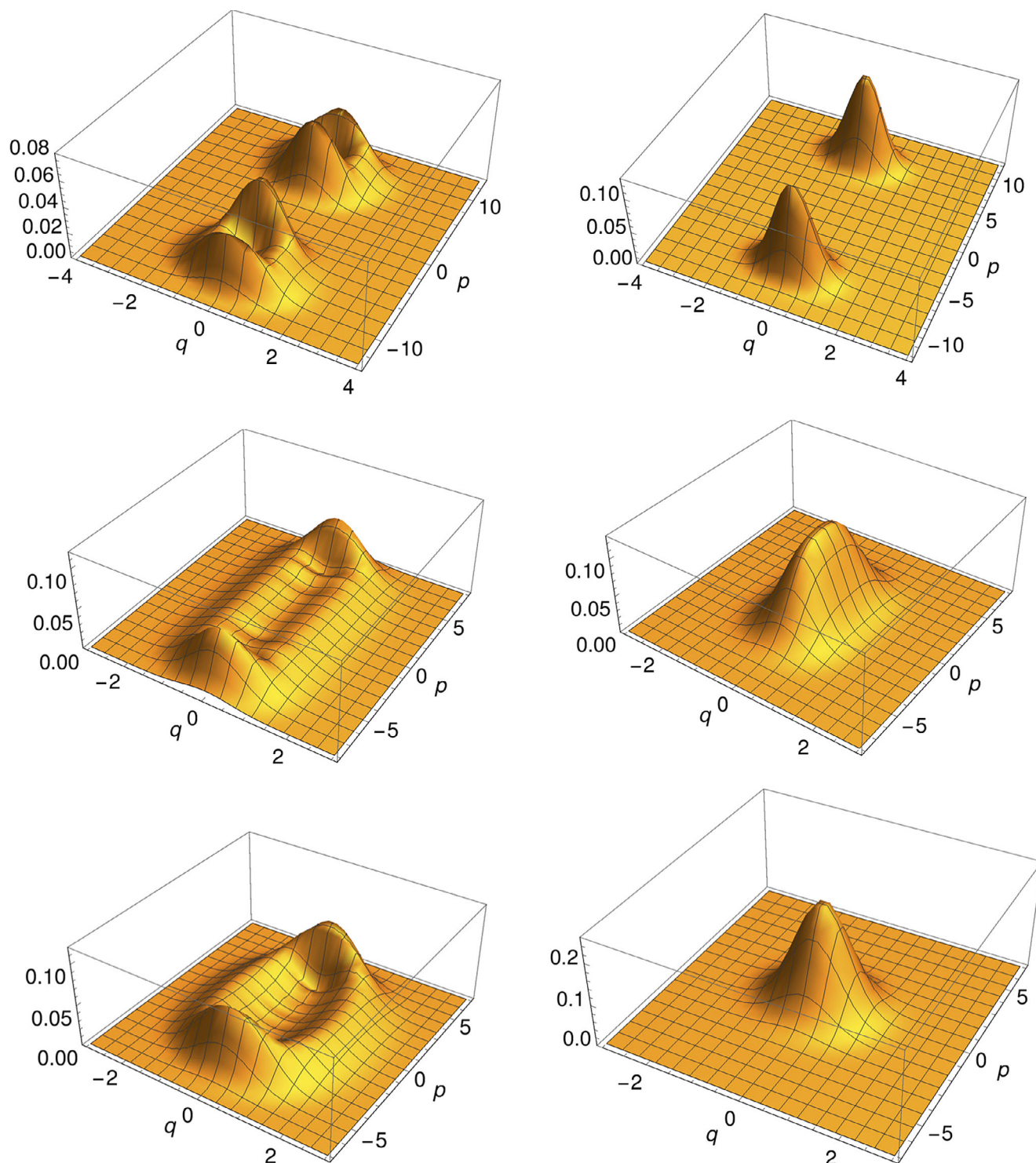
FIGURE 4 (Color online) 3D plot of the reduced Husimi distribution $Q^L_{\psi_k}(\alpha)$, as a function of $\alpha = q + ip$, for the edge state $k = 0$ (right column) and the even-parity valence band state $k = -6$ (left column) for different values of the electric potential Δ (from top to bottom): $\Delta = -1.8$ (topological insulator region), $\Delta = -1.52$ (critical), and $\Delta = -1$ (band insulator region)

1 in both sectors. Performing the integrals (20) for a Hamiltonian eigenstate (7), we arrive at an explicit formula for the normalized IPR in the Landau sector

$$P^L_k = \sum_{\substack{n,\bar{n} \\ n',\bar{n}'}} \sum_{s,s'} \frac{(n+n')! c^{(k)}_{ns} \bar{c}^{(k)}_{\bar{n}s} c^{(k)}_{n's'} \bar{c}^{(k)}_{\bar{n}'s'}}{2^{n+n'}(n!\bar{n}!n'!\bar{n}'!)^{1/2}} \delta_{n+n',\bar{n}+\bar{n}'} \tag{23}$$

FIGURE 5 Reduced Husimi distribution $Q_{\psi_k}^B(\theta)$ for the valence-band state $k = -6$, the edge state $k = 0$, and the conduction band state $k = +6$, for different values of the electric potential: $\Delta = -1.8$ (topological-insulator region, dashed line), $\Delta = -1.52$ (critical point, solid line), and $\Delta = -1$ (band insulator region, dotted line)
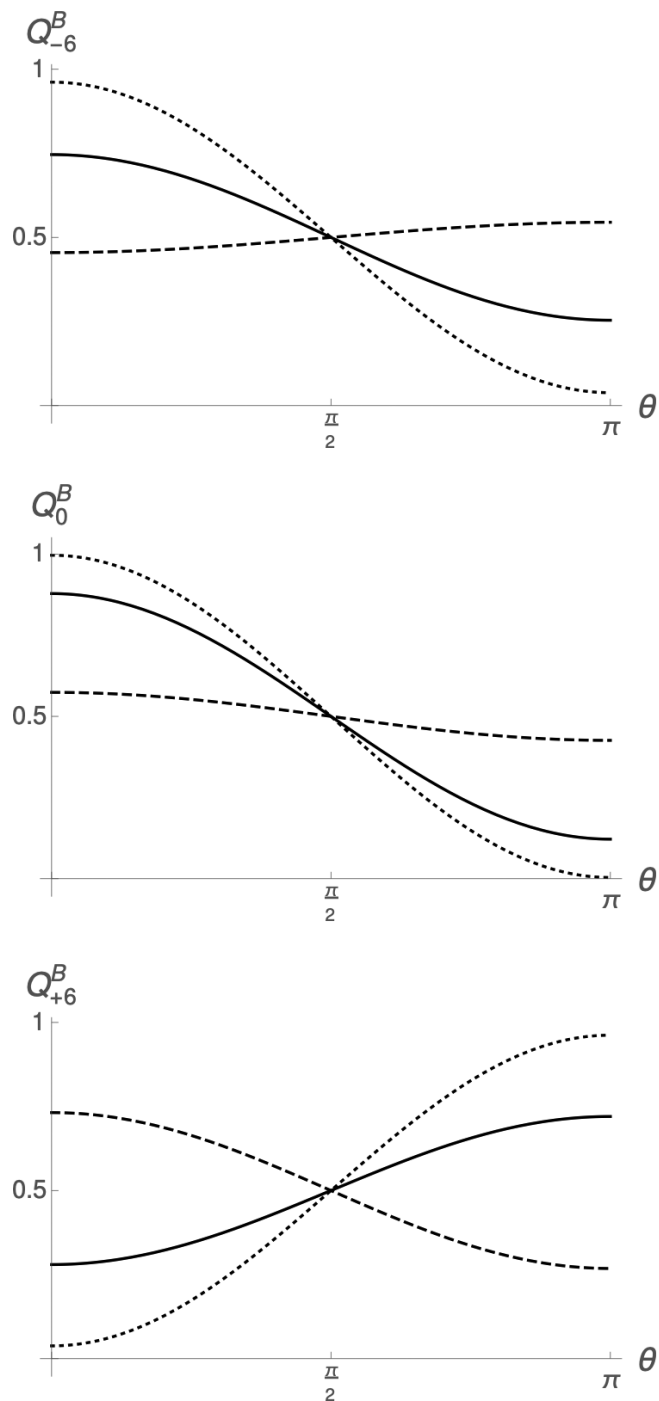
and in the band sector

$$P_k^B = \varrho_{++}^2 + \varrho_{--}^2 + \varrho_{++}\varrho_{--} + |\varrho_{+-}|^2 \tag{24}$$

where $\varrho_{\pm\pm}$ are the components of $\left(\rho_{\psi_k}^B\right)$ in Equation (19). In Figure 6, we plot P_k^L and P_k^B as a function of the electric potential strength Δ. Notice that the maximum delocalization (minimal IPR, high entanglement) of the energy eigenvectors in phase space occurs in the TI phase ($\Delta < -1.52$ eV), whereas in the BI phase ($\Delta < -1.52$ eV), the corresponding wave functions are highly localized (maximum IPR, low entanglement). This behavior is also shared with silicene.[34,36] In fact, delocalization and entanglement in phase space turns out to also be a common feature of QPTs.[32] In fact, in the next section, we analyze the phase-space structure of normal and superradiant phases of two paradigmatic spin-boson systems (Rabi-Dicke and Jaynes-Cummings), comparing them with band and topological insulator phases of phosphorene and silicene, respectively.

6 | COMPARISON WITH RABI-DICKE AND JAYNES-CUMMINGS MODELS

In this section, we want to highlight some analogies between topological insulator and superradiant quantum phases. To this end, we shall discuss some similarities between the effective Hamiltonian (2 and 4) for phosphorene and the well-known Rabi-Dicke Hamiltonian

$$\widehat{H}_R = \hbar\omega_0\frac{\sigma_z}{2} + \hbar\omega\widehat{a}^\dagger\widehat{a} + \frac{\hbar\Omega}{2}\left(\widehat{a}+\widehat{a}^\dagger\right)(\sigma_+ + \sigma_-), \tag{25}$$

originally introduced in the context of nuclear magnetic spin resonance but later extended to modeling the interaction (with coupling strength Ω) of a two-level system (spin, atoms, superconducting qubits, etc.) of transition frequency ω_0 with a harmonic oscillator (electromagnetic field, resonator, phonons, etc.) of cavity frequency ω. As for phosphorene, Rabi-Dicke Hamiltonian also conserves the parity $\pi(n,s) = e^{i\pi n_s}$ of the state $|n, s\rangle$, with $n_s = n + (s + 1)/2$, as the parity operator $\widehat{\Pi} = e^{i\pi\widehat{n}_\sigma}$, with $\widehat{n}_\sigma = \widehat{n} + (\sigma_z + \sigma_0)/2$, also commutes with $\widehat{H}_R$. When quickly oscillating "counter-rotating" terms $\widehat{a}^\dagger\sigma_+$ and $\widehat{a}\sigma_-$ are ignored ("rotating-wave approximation"), the Rabi-Dicke Hamiltonian becomes the Jaynes-Cummings Hamiltonian

$$\widehat{H}_{JC} = \hbar\omega_0\frac{\sigma_z}{2} + \hbar\omega\widehat{a}^\dagger\widehat{a} + \frac{\hbar\Omega}{2}\left(\widehat{a}\sigma_+ + \widehat{a}^\dagger\sigma_-\right), \tag{26}$$

which now also conserves the number of excitations $\widehat{n}_\sigma = \widehat{n} + (\sigma_z + \sigma_0)/2$, and not only the parity $\widehat{\Pi}$, just like the silicene Hamiltonian (5) does. This conservation law leads to a U(1)-continuous symmetry. As for silicene, this case is far simpler, and the diagonalization can be done in the subspaces $\mathscr{H}_n = \{|n, 1\rangle, |n + 1, -1\rangle\}$, with the energy eigenvalues being

$$E_n^\pm = \hbar\omega\left(n + \frac{1}{2}\right) \pm \frac{1}{2}\hbar\sqrt{\delta^2 + \Omega^2(n+1)}, \tag{27}$$

where $\delta = \omega_0 - \omega$ is the detuning parameter. The Hamiltonian eigenstates are
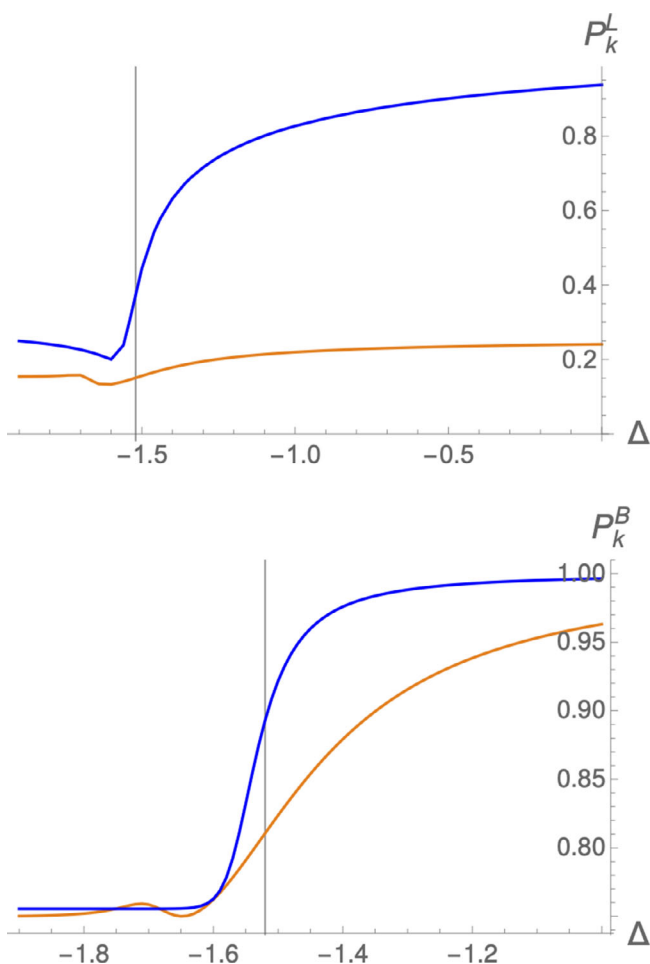
FIGURE 6 Normalized inverse participation ratios (IPRs) P_k^L and P_k^B as a function of the electric potential strength Δ for the edge state $k = 0$ (in blue) and the even-parity valence band state $k = -6$ (in orange). The critical point $\Delta_c = -1.52$ eV, separating the band from the topological insulator regime, is marked with a vertical grid line

$$|\psi_n^{\pm}\rangle = \cos\frac{\varphi_n}{2}|n + \frac{1\mp1}{2}, \pm1\rangle \pm \sin\frac{\varphi_n}{2}|n + \frac{1\pm1}{2}, \mp1\rangle,\tag{28}$$

where $\varphi_n = \arctan\frac{\Omega\sqrt{n+1}}{\delta}$. Note the similarities between this case and the silicene Hamiltonian eigenvalues (8) and eigenstates (9), although here, n is restricted to nonnegative numbers, $n \geq 0$, due to the presence of $\hbar\omega\hat{a}^{\dagger}\hat{a}$ in the Hamiltonian.

When we have an ensemble of N identical two-level atoms, the Rabi-Dicke Hamiltonian becomes the Dicke Hamiltonian by replacing $\sigma_{\pm} \rightarrow J_{\pm}/\sqrt{N}$, where $J_{\pm}$ are angular momentum ladder operators for a pseudospin $j = N/2$. In the thermodynamic limit $N \rightarrow \infty$, and at a critical value $\Omega_c = \sqrt{\omega_0\omega}$ of the atom-field coupling strength Ω, this system undergoes a QPT from a normal ($\Omega < \Omega_c$) to a superradiant ($\Omega > \Omega_c$) phase. For finite values of N, we still can observe precursors of this QPT.

Our two-band model of phosphorene shares many similarities with the Dicke model for $N = 1$, $j = 1/2$ (ie, the Rabi-Dicke model). Actually, there is a parallelism between the TI phase of phosphorene and the superradiant phase of the atom-field system. In fact, the phase-space structure of edge states turns out to be similar to the ground-state structure of the atom-field system across the critical point. Coherent states prove to be an excellent variational approximation of the ground state in QPTs. Let us denote for simplicity $|z\rangle = |\theta, \phi\rangle$, $z = \tan(\theta/2)e^{i\phi}$ the coherent state (13). Using the direct product $|\alpha, z\rangle \equiv |\alpha\rangle \otimes |z\rangle$ as a ground-state ansatz for the Rabi-Dicke Hamiltonian (25), one can easily compute the mean energy

$$\begin{aligned}H(\alpha,z) &= \langle\alpha,z|H|\alpha,z\rangle\\ &= \omega|\alpha|^2 + j\omega_0\frac{|z|^2-1}{|z|^2+1} + \Omega(\alpha + \bar{\alpha})\frac{\bar{z}+z}{|z|^2+1},\end{aligned}\tag{29}$$

which defines a four-dimensional "energy surface." Minimizing with respect to these four (two complex z, α) coordinates gives the equilibrium points:

$$\alpha_0 = \begin{cases} 0, & \text{if } \Omega < \Omega_c,\\ -\sqrt{\frac{\omega_0}{\omega}}\frac{1}{\Omega\Omega_c}\sqrt{\Omega^4 - \Omega_c^4}, & \text{if } \Omega \geq \Omega_c \end{cases}$$
$$z_0 = \begin{cases} 0, & \text{if } \Omega < \Omega_c,\\ \sqrt{\frac{\Omega^2 - \Omega_c^2}{\Omega^2 + \Omega_c^2}}, & \text{if } \Omega \geq \Omega_c, \end{cases}\tag{30}$$

together with $-\alpha_0$ and $-z_0$. Note that α_0 and z_0 are real and nonzero above the critical point Ω_c (ie, in the superradiant phase). The existence of two solutions, (α_0, z_0) and $(-\alpha_0, -z_0)$, indicates that the ground state is degenerate in the superradiant phase. This is related to the parity symmetry $\hat{\Pi}$ of the Hamiltonian (25). Therefore, the variational approximation to the ground state is a (even) parity-adapted coherent state

$$|\psi_0\rangle = \frac{|\alpha_0\rangle \otimes |z_0\rangle + |-\alpha_0\rangle \otimes |-z_0\rangle}{\mathcal{N}(\alpha_0, z_0)},\tag{31}$$

where

$$\mathcal{N}(\alpha_0, z_0) = \sqrt{2}\left(1 + e^{-2|\alpha_0|^2}\left(\frac{1 - |z_0|^2}{1 + |z_0|^2}\right)^{2j}\right)^{1/2}\tag{32}$$

is a normalization factor. This parity-adapted coherent state is also called a "Schrödinger's cat state" in the literature, in the sense that it is a quantum superposition of two quasiclassical, macroscopically distinguishable states.[56]

Taking into account the coherent state overlaps

$$\begin{aligned}\langle\alpha|\pm\alpha_0\rangle &= e^{-\frac{1}{2}|\alpha| - \frac{1}{2}\alpha_0^2 \pm \bar{\alpha}\alpha_0},\\ \langle z|\pm z_0\rangle &= \frac{(1 \pm \bar{z}z_0)^{2j}}{\left(1 + |z|^2\right)^j\left(1 + z_0^2\right)^j},\end{aligned}\tag{33}$$

the Husimi function for the variational ground states (31), $Q_0(\alpha, z) = |\langle\alpha, z|\psi_0\rangle|^2$, can be simply written as:

$$Q_0(\alpha, z) = \frac{|\langle\alpha|\alpha_0\rangle\langle z|z_0\rangle + \langle\alpha|-\alpha_0\rangle\langle z|-z_0\rangle|^2}{\mathcal{N}^2(\alpha_0, z_0)}. \tag{34}$$

A plot of this function in the normal ($\Omega < \Omega_c$) and superradiant ($\Omega < \Omega_c$) phases and at the critical point ($\Omega = \Omega_c$) can be seen in del Real et al.[20] One can appreciate the similarities between this Husimi function and the reduced Husimi distribution $Q_0^L(\alpha)$ of the edge state in Figure 4 (right panel). The normal phase of the matter-radiation system ($\Omega < \Omega_c$) corresponds to the band-insulator phase ($\Delta > \Delta_c$), where the Husimi distribution is highly localized (a single hump), whereas the superradiant phase of the atom-field system ($\Omega > \Omega_c$) corresponds to the topological-insulator phase ($\Delta < \Delta_c$), where the Husimi distribution is delocalized (two humps), displaying a Schrödinger's cat structure.

The role of Landau and band sectors in 2D Dirac materials is now played by the field and the atom sectors in the spin-boson system. References [57–60] consider the entanglement between the atoms and the field in the ground state of the Dicke model, showing that the entanglement sharply grows in the superradiant phase. In this sense, we also observe a clear analogy between the TI and the superradiant phases. Indeed, in Figure 6, we represent the purity of the reduced density matrices in the band and Landau sectors for the edge state, which shows that the edge state is far more entangled in the TI than in the BI phase. This reinforces the analogy between TI and superradiant phases.

7 | CONCLUSIONS

We have analyzed the low-energy regime of two 2D Dirac materials, phosphorene and silicene, under the influence of external perpendicular magnetic and electric fields. The electric field is used to tune the band gap (Dirac mass) and to control the appearance of edge currents in the TI phase. We visualize the structure of the edge and first Landau levels using different information-theoretic measures as a function of the electric field in the vicinity of the TPT. In particular, we use a representation of edge and first LL states in terms of coherent states in phase space (the Husimi function). We show that the entanglement between the band and Landau sectors is much higher in the TI phase. Under this perspective, we evidence a close analogy between the TI phase of 2D Dirac materials (in particular, phosphorene and silicene) and the superradiant phase of atom-field interaction systems (in particular, the Rabi-Dicke and Jaynes-Cummings models).

This semiclassical phase-space picture and information-theoretic analysis of quantum and TPTs offers a new and alternative vision that can be extrapolated to general TIs and spin-boson systems. We believe that our approach is better than existing ones in describing the electronic structure of 2D TIs in the sense that it reveals clear connections with standard QPTs, where the extensive literature and existing knowledge can help to better understand the more novel topological case. These analogies can lead to propose experimental counterparts of relevant phenomena observed in atom-field critical quantum systems, like wave packet revivals, superradiance, and—in general—about the temporal evolution of quantum correlation measures. In addition, we also believe that this vision could provide a better understanding of the relevant experimental observations of topological phases reported so far from a different perspective. This is work in progress.

AUTHOR CONTRIBUTIONS

Manuel Calixto: Investigation; writing-original draft. Elvira Romera: Investigation. Octavio Castaños: Investigation.

ORCID

Manuel Calixto https://orcid.org/0000-0002-2566-9590
Elvira Romera https://orcid.org/0000-0002-8088-9887
Octavio Castaños https://orcid.org/0000-0003-2514-3764

REFERENCES

[1] S. Sachdev, *Quantum Phase Transitions*, 2nd ed., Cambridge University Press, New York **2011** ISBN 978-0-521-51468-2.
[2] L. D. Carr, , *Understanding Quantum Phase Transitions*, CRC Press, Boca Raton **2010** ISBN 978-1-4398-0251-9.
[3] E. T. Jaynes, F. W. Cummings, *Proc. IEEE.* **1963**, *51*, 89.
[4] A. D. Greentree, J. Koch, J. Larson, (Editors)*J. Phys. B* **2013**, *46*, 22.
[5] S.-Q. Shen, *Topological Insulators: Dirac Equation in Condensed Matters*, Springer-Verlag, Berlin Heidelberg **2012**.
[6] B. A. Bernevig, (with T. L. Hughes)*Topological Insulators and Topological Superconductors*, Princeton University Press, Princeton and Oxford **2013**.

[7] J. K. Asbóth, L. Oroszlány, A. Pályi, *A Short Course on Topological Insulators: Band Structure and Edge States in One and Two Dimensions*, Springer International Publishing Switzerland, Heidelberg **2016**.

[8] M. J. S. Spencer, T. Morishita, *Mater. Sci.* **2016**, *235*, 1.

[9] A. Carvalho, M. Wang, X. Zhu, A. S. Rodin, H. Su, A. H. Castro-Neto, *Nat. Rev. Mater.* **2016**, *1*, 1.

[10] R. Wan, X. Cao, J. Guo, *Appl. Phys. Lett.* **2014**, *105*, 163511.

[11] H. Liu, Y. Du, Y. Deng, P. D. Ye, *Chem. Soc. Rev.* **2015**, *44*, 2732.

[12] M. Akhtar, G. Anderson, R. Zhao, A. Alruqi, J. E. Mroczkowska, G. Sumanasekera, J. B. Jasinski, *NPJ 2D Mater. Appl.* **2017**, *1*, 5.

[13] L. Li, Y. Yu, G. J. Ye, Q. Ge, X. Ou, H. Wu, D. Feng, X. H. Chen, Y. Zhang, *Nat. Nanotechnol.* **2014**, *9*, 372.

[14] P. Chen, N. Li, X. Chen, W. J. Ong, X. Zhao, *2D Mater* **2017**, *5*, 014002.

[15] X. Ling, H. Wang, S. Huang, F. Xia, M. S. Dresselhaus, *Proc. Natl. Acad. Sci. USA* **2015**, *112*, 4523.

[16] R. Xu, S. Zhang, F. Wang, J. Yang, Z. Wang, J. Pei, Y. W. Myint, B. Xing, Z. Yu, L. Fu, Q. Qin, Y. Lu, *ACS Nano* **2016**, *10*, 2046.

[17] E. Romera, M. Calixto, Á. Nagy, *EPL* **2012**, *97*, 20011.

[18] Á. Calixto, I. Nagy, I. Paradela, E. Romera, *Phys. Rev* **2012**, *A85*, 053813.

[19] E. Romera, R. del Real, M. Calixto, *Phys. Rev* **2012**, *A85*, 053831.

[20] R. del Real, M. Calixto, E. Romera, *Phys. Scr.* **2013**, *T153*, 014016.

[21] M. Calixto, R. del Real, E. Romera, *Phys. Rev* **2012**, *A86*, 032508.

[22] M. Calixto, E. Romera, R. del Real, *J. Phys. A (Math. & Theor.)* **2012**, *45*, 365301.

[23] M. Calixto, F. Pérez-Bernal, *Phys. Rev. A* **2014**, *89*, 032126.

[24] E. Romera, M. Calixto, O. Castaños, *Phys. Scr.* **2014**, *89*, 095103.

[25] M. Calixto, O. Castaños, E. Romera, *EPL* **2014**, *108*, 47001.

[26] M. Calixto, O. Castaños, E. Romera, *J. Stat. Mech.: Theory Exp.* **2017**, *2017*, 103103.

[27] E. Romera, O. Castaños, M. Calixto, F. Pérez-Bernal, *J. Stat. Mech.: Theory Exp.* **2017**, *2017*, 013101.

[28] C. Pérez-Campos, J. R. González-Alonso, O. Castaños, R. López-Peña, *Ann. Phys. (NY)* **2010**, *325*, 325.

[29] M. Calixto, C. Peón-Nieto, E. Pérez-Romero, *Phys. Rev* **2017**, *B95*, 235302.

[30] M. Calixto, C. Peón-Nieto, *J. Stat. Mech.: Theory Exp.* **2018**, *2018*, 053112.

[31] M. Calixto, C. Peón-Nieto, E. Pérez-Romero, *Ann. Phys.* **2016**, *373*, 52.

[32] O. Castaños, M. Calixto, F. Pérez-Bernal, E. Romera, *Phys. Rev* **2015**, *E92*, 052106.

[33] O. Castaños, E. Romera, M. Calixto, *Mater. Res. Express* **2019**, *6*, 106316.

[34] M. Calixto, E. Romera, *EPL* **2015**, *109*, 40003.

[35] E. Romera, M. Calixto, *J. Phys.: Condens. Matter* **2015**, *27*, 175003.

[36] M. Calixto, E. Romera, *J. Stat. Mech.* **2015**, P06029. https://doi.org/10.1088/1742-5468/2015/06/P06029

[37] E. Romera, M. Calixto, J. C. B. Fernández, *Phys. A* **2018**, *511*, 174.

[38] D. Corbridge, *Phosphorus: Chemistry, Biochemistry and Technology*, 6th ed., CRC Press, Boca Raton **2013**.

[39] P. W. Bridgman, *J. Am. Chem. Soc.* **1914**, *36*, 1344.

[40] P. W. Bridgman, *J. Am. Chem. Soc.* **1916**, *38*, 609.

[41] Z. Zhu, D. Tománek, *Phys. Rev. Lett.* **2014**, *112*, 176802.

[42] H. Guo, N. Lu, J. Dai, X. Wu, X. C. Zeng, *J. Phys. Chem. C* **2014**, *118*, 14051.

[43] J. Guan, Z. Zhu, D. Tománek, *Phys. Rev. Lett.* **2014**, *113*, 046804.

[44] A. S. Rodin, A. Carvalho, A. H. Castro Neto, *Phys. Rev. Lett.* **2014**, *112*, 176801.

[45] H. Liu, A. T. Neal, Z. Zhu, Z. Luo, X. Xu, D. Tománek, P. D. Ye, *ACS Nano* **2014**, *8*, 4033.

[46] A. N. Rudenko, M. I. Katsnelson, *Phys. Rev. B* **2014**, *89*, 201408.

[47] M. Ezawa, *New J. Phys.* **2014**, *16*, 115004.

[48] X. Y. Zhou, R. Zhang, J. P. Sun, Y. L. Zou, D. Zhang, W. K. Lou, F. Cheng, G. H. Zhou, F. Zhai, K. Chang, *Sci. Rep.* **2015**, *5*, 12295.

[49] L. Stille, C. J. Tabert, E. J. Nicol, *Phys. Rev. B* **2012**, *86*, 195405.

[50] C. J. Tabert, E. J. Nicol, *Phys. Rev. Lett.* **2013**, *110*, 197402.

[51] C. J. Tabert, E. J. Nicol, *Phys. Rev. B* **2013**, *88*, 085434.

[52] M. Tahir, U. Schwingenschlögl, *Sci. Rep.* **2013**, *3*, 1075.

[53] A. Perelomov, *Generalized Coherent States and Their Applications*, Springer-Verlag, Berlin, Heidelberg **1986**.

[54] A. Wehrl, *Rep. Math. Phys.* **1979**, *16*, 353.

[55] E. H. Lieb, *Commun. Math. Phys.* **1978**, *62*, 35.

[56] O. Castaños, E. Nahmad-Achar, R. López-Peña, J. G. Hirsch, *Phys. Rev. A* **2011**, *84*, 013819.

[57] N. Lambert, C. Emary, T. Brandes, *Phys. Rev. Lett.* **2004**, *92*, 073602.

[58] N. Lambert, C. Emary, T. Brandes, *Phys. Rev. A* **2005**, *71*, 053804.

[59] O. Castaños, R. López-Peña, E. Nahmad-Achar, J. G. Hirsch, *J. Phys.: Conf. Ser.* **2012**, *403*, 012003.

[60] O. Castaños, R. López-Peña, E. Nahmad-Achar, J. G. Hirsch, *AIP Conf. Proc.* **2012**, *1488*, 138.